A study on mixed electro-osmotic/pressure driven microchannel flows of a generalised Phan-Thien–Tanner fluid

Corresponding author: angelaribau@fe.up.pt

A. M. Ribau[a], L. L. Ferrás[b], M. L. Morgado[c], M. Rebelo[d], M. A. Alves[e], F. T. Pinho[a], A. M. Afonso[a]

[a] *Centro de Estudos de Fenómenos de Transporte, Departamento de Engenharia Mecânica, Faculdade de Engenharia da Universidade do Porto, Rua Dr. Roberto Frias, s/n, 4200-465, Porto, Portugal*
[b] *Centro de Matemática - CMAT & Departamento de Matemática, Universidade do Minho, Campus de Azurém, 4800-058 Guimarães, Portugal*
[c] *Center for Computational and Stochastic Mathematics, Instituto Superior Técnico, Universidade de Lisboa & Department of Mathematics, University of Trás-os-Montes e Alto Douro, UTAD, 5001-801 Vila Real, Portugal*
[d] *Centro de Matemática e Aplicações (CMA) and Departamento de Matemática, Faculdade de Ciências e Tecnologia, Universidade NOVA de Lisboa, Quinta da Torre, 2829-516 Caparica, Portugal*
[e] *Centro de Estudos de Fenómenos de Transporte, Departamento de Engenharia Química, Faculdade de Engenharia da Universidade do Porto, Rua Dr. Roberto Frias, s/n, 4200-465, Porto, Portugal*

Abstract

This work presents new semi-analytical solutions for the combined fully-developed electro-osmotic (EO) pressure-driven flow in microchannels of viscoelastic fluids, described by the generalised Phan-Thien–Tanner model (gPTT) recently proposed by Ferrás et al. [Journal of Non-Newtonian Fluid Mechanics, 269: 88-99, 2019]. This generalised version of the PTT model presents a new function for the trace of the stress tensor - the Mittag-Leffler function - where one or two new fitting constants are considered in order to obtain additional fitting flexibility. The semi-analytical solution is obtained under sufficiently weak electric potentials that allows the Debye–Hückel approximation for the electrokinetic fields and for thin electric double layers.

Based on the solution, the effects of the various relevant dimensionless numbers are assessed and discussed, such as the influence of εWi^2, of the parameters α and β of the gPTT model, and also of $\bar{\kappa}$, the dimensionless Debye–Hückel parameter. We conclude that the new model characteristics enhance the effects of both εWi^2 and $\bar{\kappa}$ on the velocity distribution across the microchannels. The effects of a high zeta potential are also studied numerically.

Keywords: generalised simplified PTT, Mittag-Leffler, electro-osmotic flow/pressure driven flows, steric effect, high zeta potential

1. Introduction

Electro-osmosis (EO) is a flow forcing method suitable for flows through micro- and nano-devices that is particularly useful for applications in medicine, biochemistry and miniaturised industrial processes. EO relies on a basic electrokinetic phenomenon, where the flow of an electrolyte is driven by an external potential difference between the inlet and outlet of the channel, acting on ions that are imbalanced in the near-wall region of the fluid due to the interaction between the dielectric channel walls and the fluid. Specifically, these are layers of higher concentration of counter-ions within the fluid, that move under the action of the applied electric field, which then drags by viscous forces the neutral core as a solid body [1]. There is a vast literature dealing with this topic for Newtonian fluids [2–9].

As reviewed by Zhao and Yang [10], there is also a fair amount of literature dealing with electro-osmotic flows of non-Newtonian fluids (see also [11–14]).

In this work, we are interested in viscoelastic materials described by differential constitutive equations [15], which can describe accurately the real behaviour of polymer solutions. In order to reduce the computational effort needed to compute integral models, new differential model were proposed in the literature, such as the generalised Phan-Thien–Tanner (gPTT) [16–18] model that uses the Mittag-Leffler function as a function of the trace of the stress tensor (instead of the classical linear and exponential functions), together with one or two new fitting parameters in order to obtain additional fitting flexibility.

This model was previously studied for Couette and pressure driven flows, in the absence EO [28, 29], therefore this work aims to assess the influence of the new model parameters for combined electro-osmotic/pressure driven flows.

The remainder of this paper is organised as follows: the next section presents the governing equations, followed by the new analytical solution in Section 3, the discussion of the results in Section 4 and the conclusions of the paper in Section 5.

2. Formulation and governing equations

We consider a combined electro-osmotic/pressure-driven channel flow of a viscoelastic gPTT fluid in a microchannel, as shown in Fig. 1. Here x, y and z, represent the streamwise, transverse and spanwise directions, respectively, and the channel width is $2H$. We consider that the channel size in the spanwise direction is much larger than H, thus the flow can be assumed two-dimensional.

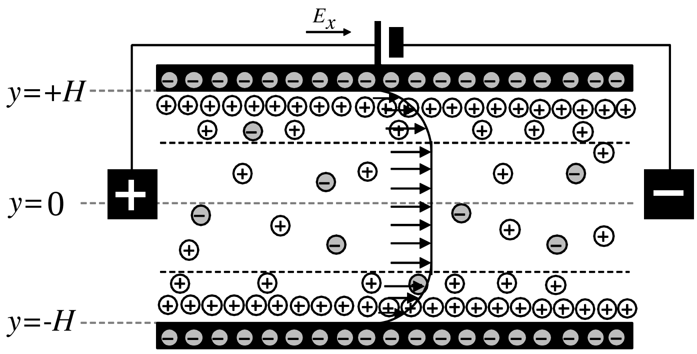

Figure 1: Schematic of the flow in a planar microchannel.

As schematically shown in Fig. 1, the ion separation arises due to the interaction between the walls and the fluid. Here, the illustrated negatively charged walls of the microchannel attract counter-ions forming layers of positively charged fluid near the walls and with the co-ions predominantly staying at the core. At such dilute concentrations, the fluid core remains essentially neutral. Very thin layers of immobile counter-ions remain at the walls, known as the Stern layers, followed by thicker more diffuse layers of mobile counter-ions; the two layers near the wall form what is called the Electrical Double Layer (EDL).

A DC potential difference between the two electrodes at the inlet and outlet generates an external electric field that exerts a body force on the counter-ions of the EDL, which flow along the channel dragging the neutral liquid core. The pressure difference that can also be applied between the inlet and outlet can act in the same direction of the electric field or in the opposite direction. At the wall, the no-slip condition applies, whereas at the centreplane the symmetry boundary condition is used. Since the flow is fully-developed, the velocity and stress fields only depend on the transverse coordinate y [11, 12].

The equations governing the flow of an isothermal incompressible fluid are the continuity equation

$$\nabla \cdot \mathbf{u} = 0, \tag{1}$$

and the momentum equation

$$\rho \frac{\mathrm{D}\mathbf{u}}{\mathrm{D}t} = -\nabla p + \nabla \cdot \boldsymbol{\tau} + \rho_e \mathbf{E}, \tag{2}$$

where $\mathbf{u}$ is the velocity vector, $\frac{\mathrm{D}}{\mathrm{D}t}$ is the material derivative, p is the pressure, t is the time, ρ is the fluid density, $\boldsymbol{\tau}$ is the extra-stress tensor, $\mathbf{E}$ is the electric field and ρ_e is the electric charge density in the fluid.

2.1. Constitutive equation

In order to achieve a closed system of equations, a constitutive equation for the extra-stress tensor, $\boldsymbol{\tau}$, is required. Recently, Ferrás et al. [18] proposed a new differential model based on the Phan-Thien–Tanner constitutive equation [16]. This new model considers a more general function for the rate of destruction of junctions, the Mittag-Leffler function, where one or two fitting parameters are included, in order to achieve additional fitting flexibility [18].

The Mittag-Leffler function is defined as,

$$E_{\alpha,\beta}(z) = \sum_{j=0}^{\infty} \frac{z^j}{\Gamma(\alpha j + \beta)}, \tag{3}$$

with α, β being real and positive. When $\alpha = \beta = 1$, the Mittag-Leffler function reduces to the exponential function, and when $\beta = 1$ the original one-parameter Mittag-Leffler function, E_α is obtained.

The constitutive equation is given by:

$$K(\tau_{kk})\, \boldsymbol{\tau} + \lambda \overset{\square}{\boldsymbol{\tau}} = 2\eta_p \mathbf{D}, \tag{4}$$

where τ_{kk} is the trace of the stress tensor, λ is the a relaxation time, η_p is the polymeric viscosity coefficient, $\mathbf{D}$ is the rate of deformation tensor and $\overset{\square}{\boldsymbol{\tau}}$ represents the Gordon-Schowalter derivative defined as

$$\overset{\square}{\boldsymbol{\tau}} = \frac{\partial \boldsymbol{\tau}}{\partial t} + \mathbf{u} \cdot \nabla \boldsymbol{\tau} - (\nabla \mathbf{u})^T \cdot \boldsymbol{\tau} - \boldsymbol{\tau} \cdot (\nabla \mathbf{u}) + \xi (\boldsymbol{\tau} \cdot \mathbf{D} + \mathbf{D} \cdot \boldsymbol{\tau}). \tag{5}$$

Here $\nabla \mathbf{u}$ is the velocity gradient and the parameter ξ accounts for the slip between the molecular network and the continuous medium. The stress function, $K(\tau_{kk})$, is given by a new formulation that imparts more flexibility and accuracy to the model predictions, as discussed in [18]. Specifically, it is given by:

$$K(\tau_{kk}) = \Gamma(\beta)\, E_{\alpha,\beta}\left(\frac{\varepsilon \lambda}{\eta_p} \tau_{kk}\right), \tag{6}$$

where ε represents the extensibility parameter, Γ is the Gamma function and the normalization $\Gamma(\beta)$ is used to ensure that $K(0) = 1$, for all choices of β.

2.2. Electric potential

We can relate the electrostatic field, $\mathbf{E}$, with the electric potential, Φ, through:

$$\mathbf{E} = -\nabla \Phi \tag{7}$$

where Φ is governed by:

$$\nabla^2 \Phi = -\frac{\rho_e}{\epsilon} \tag{8}$$

with ϵ representing the dielectric constant of the solution. The electric potential includes two different contributions, $\Phi = \phi + \psi$, where ϕ is generated by the electrodes, placed at the inlet and outlet of the flow geometry, and ψ is associated with the charge distribution near the walls. In this way, the imposed potential is described by a Laplace equation, $\nabla^2\phi = 0$, and the induced potential is described by a Poisson equation:

$$\nabla^2\psi = -\frac{\rho_e}{\epsilon}. \tag{9}$$

In some situations, such as when the flow and the ion distributions are fully-developed, the EDLs are thin and do not overlap at the centre of the channel. Significant variations of ψ only occur in the transverse direction, and a stable Boltzmann distribution of ions occurs in the EDL. Therefore, the net electric charge density, ρ_e, for an electrolyte in equilibrium near a charged surface is given by the following Boltzmann distribution [1]:

$$\rho_e = -2n_0 ez \sinh\left(\frac{ez}{k_B T}\psi\right), \tag{10}$$

where n_0 is the ion density, e the elementary charge, z the valence of the ions, T the absolute temperature and k_B the Boltzmann constant.
Combining Eq. (9) for the induced potential equation, that for fully-developed steady flow becomes,

$$\frac{\mathrm{d}^2\psi}{\mathrm{d}y^2} = -\frac{\rho_e}{\epsilon}, \tag{11}$$

with Eq. (10), leads to the Poisson-Boltzmann equation:

$$\frac{\mathrm{d}^2\psi}{\mathrm{d}y^2} = \frac{2n_0 ez}{\epsilon}\sinh\left(\frac{ez}{k_B T}\psi\right). \tag{12}$$

Assuming the Debye-Hückel linearization principle, a valid approximation provided for small values of ψ [11, 12, 32], the Poisson-Boltzmann equation (Eq. (12)) for the, 2D channel flow becomes,

$$\frac{\mathrm{d}^2\psi}{\mathrm{d}y^2} = \kappa^2\psi, \tag{13}$$

where $\kappa^2 = 2n_0 e^2 z^2/\epsilon k_B T$ is the Debye-Hückel parameter, which is related to the thickness of the Debye layer, $\lambda_D = 1/\kappa$, also called the EDL thickness.
The boundary conditions for the Poisson-Boltzmann equation are the following: at the symmetry plane, $\frac{\mathrm{d}\psi}{\mathrm{d}y}|_{y=0} = 0$; the zeta potential at the wall is $\psi_{wall} = \psi_0$. Integrating Eq. (13) and applying these boundary conditions, leads to the following induced electric field, ψ:

$$\psi(y) = \psi_0 \frac{\cosh(\kappa y)}{\cosh(\kappa H)}, \tag{14}$$

for $0 \leq y \leq H$ and $\psi(H) = \psi_0$. The electric charge density, ρ_e is given by:

$$\rho_e = -\epsilon\psi_0\kappa^2 \frac{\cosh(\kappa y)}{\cosh(\kappa H)}. \tag{15}$$

It should be remarked that the non-dimensionalization of the Nernst-Planck equation which governs the transport of ionic species shows that the relative contribution of the advective strength of the ionic species compared to diffusive strength results in the ionic Peclet number, which can be expressed as $\frac{u_{ref}H}{D}$, where u_{ref} is reference velocity, H is reference length scale (the half width of the channel) and D is the ionic diffusivity. For electro-osmotic flows, a typical velocity scale is $u_{ref} \sim \frac{\epsilon\psi_0 E_x}{\eta_p}$. Taking a viscoelastic fluid as a medium with $\epsilon \sim 10^{-9}$ C/Vm, $\eta_p \sim 10^{-2}$ Pa.s, for an electric field of $E_x \sim 10^4$ V/m and for $\psi_0 \sim 20$ mV, we obtain $u_{ref} \sim 10^{-8}$ m/s. Now, with a channel height of $2H \sim 10$ μm and $D \sim 10^{-8}$ m^2/s (typical values of ionic diffusivity), the ionic Peclet number is of order $Pe \sim 0.01$, i.e., the contribution of advection on the space distribution of ionic charges can be neglected in the present analysis, when considering the Debye–Hückel approximation.

More details regarding the derivation of these equations can be seen in Afonso et al. [11], Mondal et al. [22] and Mukherjee et al. [23].

3. Analytical solution for the gPTT model

In this section, we derive the analytical solution for the gPTT model considering fully-developed electro-osmotic/pressure-driven flow (cf. Fig.1).

The momentum equation, Eq. (2), becomes:

$$\frac{\mathrm{d}\tau_{xy}}{\mathrm{d}y} = P_x - \rho_e E_x, \tag{16}$$

where $P_x \equiv \frac{\mathrm{d}p}{\mathrm{d}x}$ is the constant streamwise pressure gradient, τ_{xy} the shear stress and $E_x \equiv \frac{\mathrm{d}\phi}{\mathrm{d}x}$ is the imposed constant streamwise gradient of electric potential. This equation is valid regardless of the rheological constitutive equation.

Now, using Eq. (15) and considering that the shear stress at the centreline is zero, Eq. (16) can be integrated leading to the following shear stress distribution:

$$\tau_{xy} = \epsilon\psi_0 E_x \kappa \frac{\sinh(\kappa y)}{\cosh(\kappa H)} + P_x y. \tag{17}$$

The constitutive equation for the gPTT model for this flow (Section 2.1) can be further simplified, leading to:

$$K(\tau_{kk})\tau_{xx} = (2-\xi)(\lambda\dot{\gamma})\tau_{xy}, \tag{18}$$

$$K(\tau_{kk})\tau_{yy} = -\xi(\lambda\dot{\gamma})\tau_{xy}, \tag{19}$$

$$K(\tau_{kk})\tau_{xy} = \eta_p\dot{\gamma} + (1-\frac{\xi}{2})(\lambda\dot{\gamma})\tau_{yy} - \frac{\xi}{2}(\lambda\dot{\gamma})\tau_{xx}, \tag{20}$$

where the velocity gradient $\dot{\gamma}$ is a function of y ($\dot{\gamma}(y) \equiv \frac{\mathrm{d}u}{\mathrm{d}y}$) and $\tau_{kk} = \tau_{xx} + \tau_{yy} + \tau_{zz}$ is the trace of the stress tensor. Under these conditions $\tau_{zz} = 0$.

3.1. Electro-Osmotic Flow with $\xi = 0$

In order to obtain closed form analytical solutions the slip parameter in the Gordon-Schowalter derivative is set to $\xi = 0$.

Assuming $\xi = 0$ Eq. (19) implies that $\tau_{yy} = 0$, and the trace of the stress tensor becomes $\tau_{kk} = \tau_{xx}$. Dividing Eq. (18) by Eq. (20), $K(\tau_{xx})$ cancels out, and an explicit relationship between the streamwise normal stress and the shear stress is found:

$$\tau_{xx} = 2\frac{\lambda}{\eta_p}\tau_{xy}^2. \tag{21}$$

Now combining Eqs. (20), (21), (17) and (6) the following velocity gradient profile is obtained,

$$\dot{\gamma}(y) = \frac{\Gamma(\beta)}{\eta_p} E_{\alpha,\beta}\left(\frac{2\varepsilon\lambda^2}{\eta_p^2}\left(\epsilon\psi_0 E_x\kappa\frac{\sinh(\kappa y)}{\cosh(\kappa H)} + P_x y\right)^2\right)\left(\epsilon\psi_0 E_x\kappa\frac{\sinh(\kappa y)}{\cosh(\kappa H)} + P_x y\right). \tag{22}$$

The dimensionless velocity gradient becomes:

$$\frac{\mathrm{d}\bar{u}}{\mathrm{d}\bar{y}} = \Gamma(\beta) E_{\alpha,\beta} \left(\frac{2\varepsilon Wi^2}{\bar{\kappa}^2} \left(\Upsilon \bar{y} - \bar{\kappa} \frac{\sinh(\bar{\kappa}\bar{y})}{\cosh(\bar{\kappa})} \right)^2 \right) \left(\Upsilon \bar{y} - \bar{\kappa} \frac{\sinh(\bar{\kappa}\bar{y})}{\cosh(\bar{\kappa})} \right), \tag{23}$$

where $Wi = \lambda \kappa u_{sh}$ is the Weissenberg number and u_{sh} is the Helmholtz-Smoluchowski electro-osmotic velocity, defined as $u_{sh} = -\frac{\epsilon \psi_0 E_x}{\eta_p}$, $\bar{u} = \frac{u}{u_{sh}}$, $\bar{y} = \frac{y}{H}$ and $\bar{\kappa} = \kappa H$. The non-dimensional parameter $\Upsilon = -\frac{H^2}{\epsilon \psi_0} \left(\frac{P_x}{E_x} \right)$ represents the ratio of pressure to electro-osmotic driving forces.
Eq. (23) has an analytical solution only for pure electro-osmotic (EO) flow and provided further assumptions are made, whereas for the combined situation with a pressure gradient (EO+PD) the solution is obtained numerically. Next, we obtain the analytical solution for pure EO, discuss its validity in Section 4, where the combined solution (EO+PD) is also discussed.

For pure EO flow, $\Upsilon = 0$, therefore the velocity profile can be obtained integrating the velocity gradient profile, subjected to the no-slip boundary condition at the top (+) or bottom (-) walls, $\bar{u}(\bar{y} = \pm 1) = 0$. Simplifying Eq. (23), the equation to be integrated is:

$$\bar{u}(\bar{y}) = -\int_{\bar{y}}^{1} \left(-\Gamma(\beta)\bar{\kappa} \sum_{j=0}^{\infty} \left(2\varepsilon Wi^2 \right)^j \left(\frac{\sinh(\bar{\kappa} z)}{\cosh(\bar{\kappa})} \right)^{2j+1} \frac{1}{\Gamma(\alpha j + \beta)} \right) \mathrm{d}z. \tag{24}$$

In order to compute the integral in (24) we consider $\sinh(\bar{\kappa}\bar{y}) \approx \frac{1}{2}\exp(\bar{\kappa}\bar{y})$ which is usually accurate because in most micro-devices, the thickness of the EDL is very small, about 1 to 3 orders of magnitude smaller than the width of the micro channel, so $\bar{\kappa}$ is a large value. However, close to the centreline the approximation ($\bar{y} \sim 0$) becomes less adequate (in this case we can use the trapezoidal rule, leading to the Crank-Nicolson method to obtain the approximate solution of the differential equation).
Assuming $\sinh(\bar{\kappa} z) \approx \frac{1}{2}\exp(\bar{\kappa} z), \quad z \in (\bar{y}, 1)$, the integration (Eq. (24)) gives the following velocity profile:

$$\bar{u}(\bar{y}) \approx -\frac{\Gamma(\beta)}{2\cosh(\bar{\kappa})} \sum_{j=0}^{\infty} \left(\frac{\varepsilon Wi^2}{2\cosh^2(\bar{\kappa})} \right)^j \frac{\left((\exp(\bar{\kappa}\bar{y}))^{2j+1} - (\exp(\bar{\kappa}))^{2j+1} \right)}{2j+1} \frac{1}{\Gamma(\alpha j + \beta)}. \tag{25}$$

When we consider $\alpha = \beta = 1$, Eq. (25) reduces to the one presented in Ferrás et al. [12] for pure EO flow of an exponential PTT fluid:

$$\bar{u}(\bar{y}) \approx \frac{\sqrt{\frac{\pi}{2}} \left(\mathrm{erfi}\left[\frac{B\sqrt{A}\exp(\bar{\kappa})}{\sqrt{2}} \right] - \mathrm{erfi}\left[\frac{B\sqrt{A}\exp(\bar{\kappa}|\bar{y}|)}{\sqrt{2}} \right] \right)}{2\bar{\kappa}\sqrt{A}}, \tag{26}$$

where $\mathrm{erfi}(z) = -i\mathrm{erf}(iz)$ with $\mathrm{erf}(.)$ denoting the error function, $A = \frac{\varepsilon Wi^2}{\bar{\kappa}^2}$ and $B = \frac{\bar{\kappa}}{\cosh(\bar{\kappa})}$.

3.2. *Electro-Osmotic Flow with $\xi \neq 0$*

When parameter $\xi \neq 0$ the behaviour of the solution is different and the EO flow may become unstable at a critical shear rate as previously shown by Dhinakaran et al. [32]. The system of differential equations are nonlinear and the velocity profile must be obtained numerically. By following the steps of Dhinakaran et al. [32] (their equations (12)-(22)) one can obtain the velocity gradient:

$$\frac{\mathrm{d}u}{\mathrm{d}y} = \frac{-\Gamma(\beta)E_{\alpha,\beta}\left[\frac{1}{\chi}\left(1-\sqrt{1-\left(a\lambda\kappa u_{sh}\frac{\sinh(\kappa y)}{\cosh(\kappa H)}\right)^2}\right)\right]\kappa u_{sh}\frac{\sinh(\kappa y)}{\cosh(\kappa H)}}{1-\frac{1}{2}\left(1-\sqrt{1-\left(a\lambda\kappa u_{sh}\frac{\sinh(\kappa y)}{\cosh(\kappa H)}\right)^2}\right)} \tag{27}$$

where $\chi = \frac{\xi(2-\xi)}{\varepsilon(1-\xi)}$ and $a = 2\sqrt{\xi(2-\xi)}$.

The velocity gradient can be written in dimensionaless form as,

$$\frac{\mathrm{d}\bar{u}}{\mathrm{d}\bar{y}} = \frac{-\Gamma(\beta)E_{\alpha,\beta}\left[\frac{1}{\chi}\left(1-\sqrt{1-\left(aWi\frac{\sinh(\bar{\kappa}\bar{y})}{\cosh(\bar{\kappa})}\right)^2}\right)\right]\bar{\kappa}\frac{\sinh(\bar{\kappa}\bar{y})}{\cosh(\bar{\kappa})}}{1-\frac{1}{2}\left(1-\sqrt{1-\left(aWi\frac{\sinh(\bar{\kappa}\bar{y})}{\cosh(\bar{\kappa})}\right)^2}\right)} \tag{28}$$

and then the velocity profile ($\bar{u}(\bar{y})$) can be obtained by applying to Eq. (28) a fourth-order Runge-Kutta method together with 20-30 parcels to approximate the Mittag-Leffler function.

The steric effects are presented in appendix.

4. Discussion of results

4.1. *Pure electro-osmotic flow*

Before performing a study on the influence of the different parameters on the fluid flow, we briefly discuss the validity of the approximate analytical solution given by Eq. (25). We compare in Fig. 2 the results obtained with this equation and the results obtained numerically by discretizing Eq. (24) with the Simpson's quadrature rule. For the approximation of the infinite series we performed numerical tests and observed that the use of 20-40 terms would allow us to obtain an accurate sum up to the sixth decimal place.

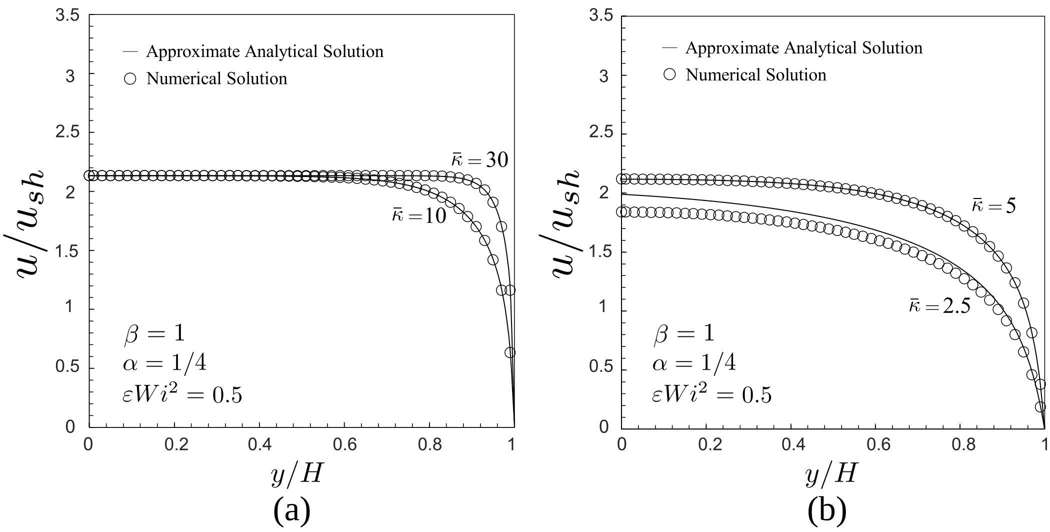

Figure 2: Velocity profiles calculated using Eqs. (25) (symbols) and (24) (lines) for the pure EO flow considering $\varepsilon Wi^2 = 0.5$ and different values of $\bar{\kappa}$ for $\alpha = 1/4$ and $\beta = 1$: (a) $\bar{\kappa} = 10$ and $\bar{\kappa} = 30$; (b) $\bar{\kappa} = 2.5$ and $\bar{\kappa} = 5$.

As expected, it can be seen that only for low values of $\bar{\kappa}$, ($\bar{\kappa} \leq 4.5$) the thin layer approximation of the analytical solution fails to predict the correct velocity profile. Therefore, the values of $\bar{\kappa}$ used along this work will be greater or equal than 10.

We will now investigate the influence of the Mittag-Leffler function parameters α and β, on the velocity profile distribution across the channel for different values of εWi^2 and $\bar{\kappa}$, and we compare the results with those for the exponential PTT model.

Fig. 3 compares the velocity profiles obtained for EO flow considering two different εWi^2 values and different values of α (Fig. 3(a)) and β (Fig. 3(b)) at $\bar{\kappa} = 10$. In Fig. 3 (a) $\beta = 1$ and we observe that for increasing εWi^2 and decreasing α the flow rate increases, which is due to enhanced shear-thinning at the shear rates prevailing within the EDL. In Fig. 3 (b) $\alpha = 1$ and a similar qualitative behaviour is obtained, i.e., on increasing εWi^2 and decreasing β, the flow rate increases. However, there are quantitative differences with the effect of β being stronger than the effect of α. Note that both α and β play a role similar to ε in the classical PTT model, that is, increasing α and β, we are increasing the net rate of destruction of network junctions in the physical model of the polymer, and therefore the fluid becomes more thinning, reducing the friction between junctions [18]. The fact that β plays a stronger role on the thinning effect comes from the fact that the new function of the trace of the stress tensor presents higher numerical values for $\beta \ll 1$ when the argument is smaller than ≈ 1 (the case of the EO flow presented here).

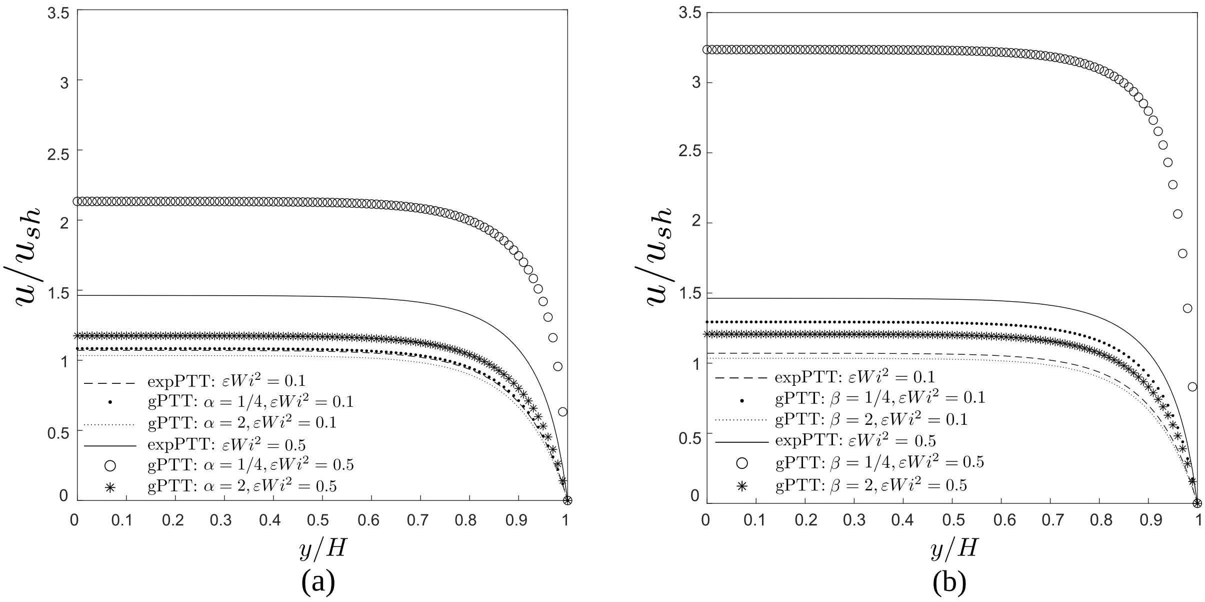

Figure 3: Velocity profiles calculated using Eq. (25) for the pure electro-osmotic flow considering different values of εWi^2 and different values of α and β for $\bar{\kappa} = 10$: (a) $\beta = 1$; (b) $\alpha = 1$. The velocity profiles were obtained from Eq. (25) and the cases for expPTT correspond to $\alpha = \beta = 1$.

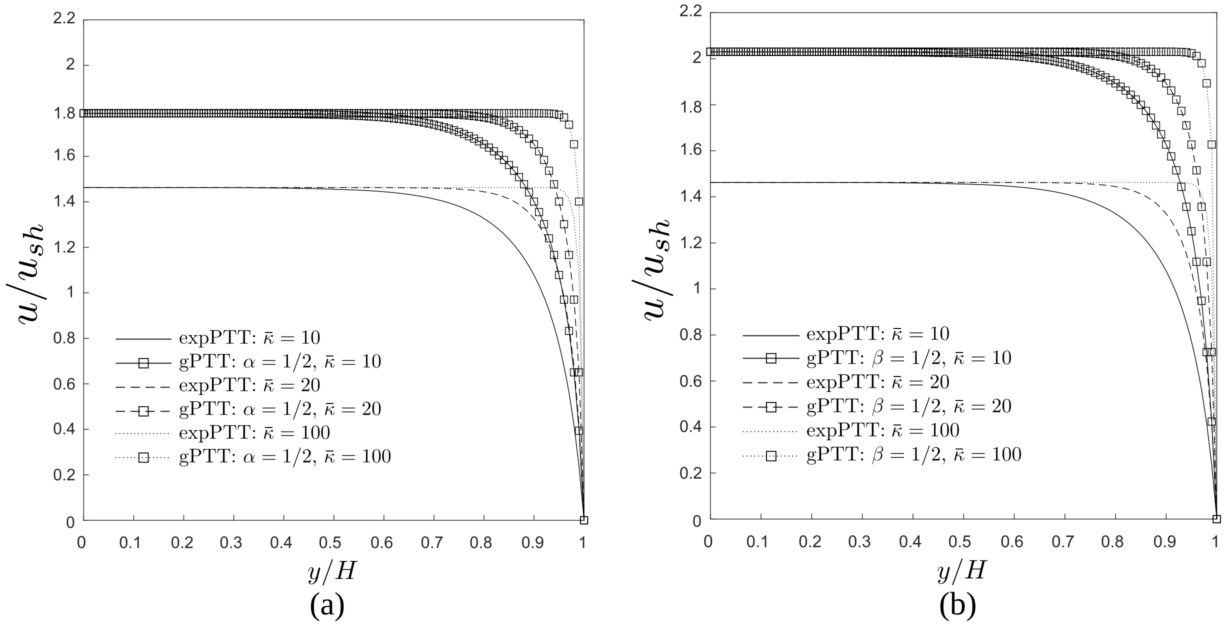

Figure 4: The effect of $\bar{\kappa}$ on transverse velocity profiles for EO at $\varepsilon Wi^2 = 0.5$: (a) $\beta = 1$; (b) $\alpha = 1$. The velocity profiles were obtained from Eq. (25) and the cases with expPTT correspond to $\alpha = \beta = 1$.

Fig. 4 compares transverse velocity profiles for the EO flow considering three different values of $\bar{\kappa}$, at fixed $\varepsilon Wi^2 = 0.5$: Fig. 4 (a) refers to fixed $\beta = 1$, and we observe the expected thinning of the EDL with increasing $\bar{\kappa}$. Similar trends are observed in Fig. 4 (b). The highest shear rates occur near the walls and in this region the effects of α and β will be felt more strongly, as discussed in [18]. Smaller values of these parameters mean that the rate of destruction of junctions increases, that is, the friction between the molecules of the polymer solution decreases, leading to a less resistive flow (stronger shear-thinning). These effects are qualitatively similar to those observed with other shear thinning fluids, even if quantitatively different. For a constant viscosity fluid the ratio between the maximum velocity (taking place on the centre plane) and the Helmholtz-Smoluchowski velocity is 1, for high $\bar{\kappa}$, but on increasing shear-thinning effects, this ratio increases, as shown in Fig. 5 (a), (b) and Fig. 6.

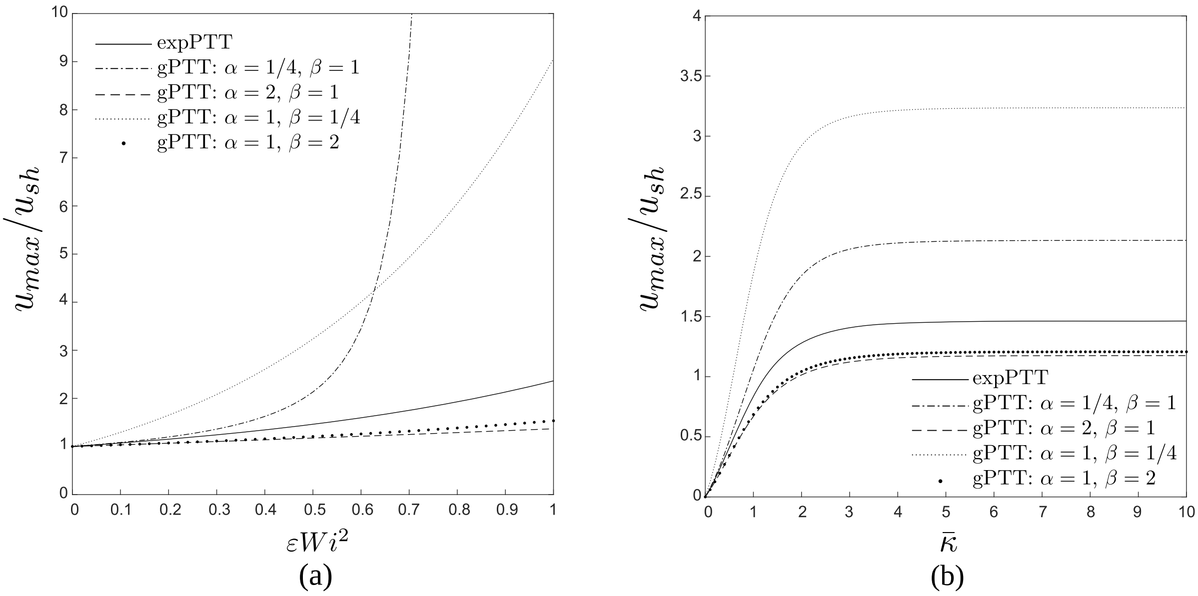

Figure 5: Ratio between maximum velocity and u_{sh} as a function of the relevant dimensionless numbers: (a) $\bar{\kappa} = 10$; (b) $\varepsilon Wi^2 = 0.5$. The velocities were obtained from Eq. (25) and the cases with expPTT correspond to $\alpha = \beta = 1$.

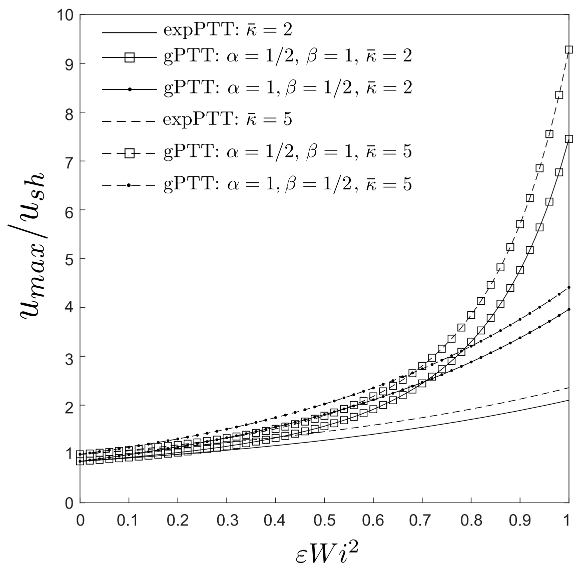

Figure 6: Ratio between maximum velocity and u_{sh} as a function of εWi^2 for different values of $\bar{\kappa}$, α and β. The velocities were obtained from Eq. (25) and the cases with expPTT correspond to $\alpha = \beta = 1$.

4.1.1. Influence of the Polymer Concentration

We consider three polyethylene oxide (PEO) solutions in a glycerol-water Newtonian solvent. The solvent viscosity is $\eta = 0.002$ Pa.s. The PEO has average molecular weight Mw = 4 MDa (Sigma-Aldrich) and the aqueous PEO solutions considered have concentrations of $c = 1$ g/l, $c = 3$ g/l and $c = 7$ g/l [19]. The experimental data (shear viscosity versus shear rate) from [19] and the fit obtained with the gPTT model are shown in Fig. 7 (a). Note that for the higher concentration it is possible to see the shear-thinning effect more noticeably.

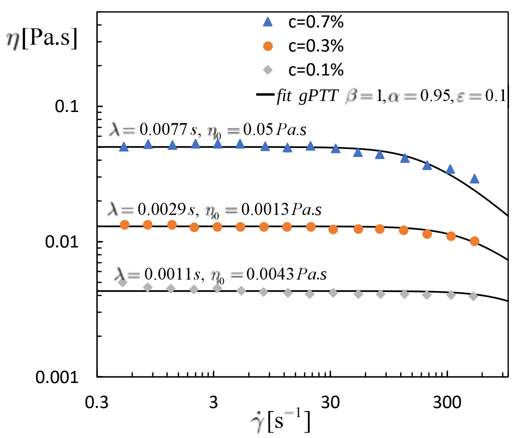

(a)

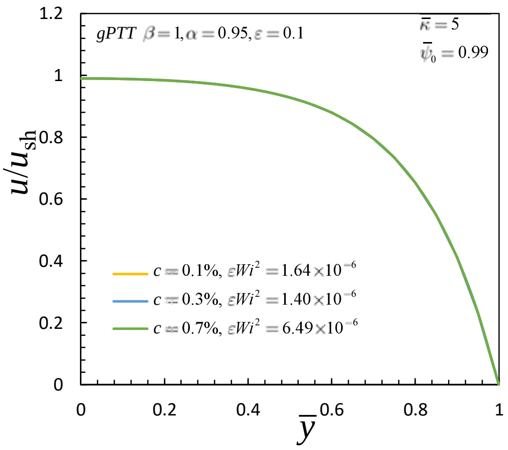

(b)

Figure 7: (a) Fit of the gPTT model to the experimental data obtained for three aqueous PEO solutions with concentrations of $c = 1$ g/l, $c = 3$ g/l and $c = 7$ g/l. (b) Pure EO flow obtained for the three aqueous solutions.

Fig. 7 (a) also shows the values of the relaxation time λ and the zero-shear viscosity η_0 obtained experimentally. A good fit was possible to obtain by considering $\alpha = 0.95$, $\beta = 1$, $\varepsilon = 0.1$ and three different values of η_0 (0.0043, 0.013 and 0.05 Pa.s).

We also plotted (Fig. 7 (b)) the velocity profiles obtained for the pure EO flow considering the rheological parameters obtained from the fit to the experimental shear viscosity. It is interesting to see that the values obtained for εWi^2 are not increasing with the polymer concentration. This is due to the definition of Wi, that takes into account the viscous and elastic effects. The values of parameters λ and η used in the definition of Wi are those obtained experimentally, and shown in Fig. 7 (a). For such low values of εWi^2 the velocity profiles are all collapsed and the flow is Newtonian-like.

It should be remarked that the λ and η parameters obtained in [19] slightly differ from the ones in [21], and therefore, the differences obtained in εWi^2 should take this into consideration. For more experimental results please see [23].

4.2. Electro-osmotic–pressure driven flow

In the case of mixed EO/PD flows ($\Upsilon \neq 0$), Eq. (23) was solved numerically, using the Runge–Kutta fourth-order order method in MATLAB software. The influence of the new model on the velocity profile was assessed considering $\Upsilon = -1$ and $\Upsilon = 1$. Numerical solution of Eq. (23) for different values for α and β are plotted in Fig. 8.

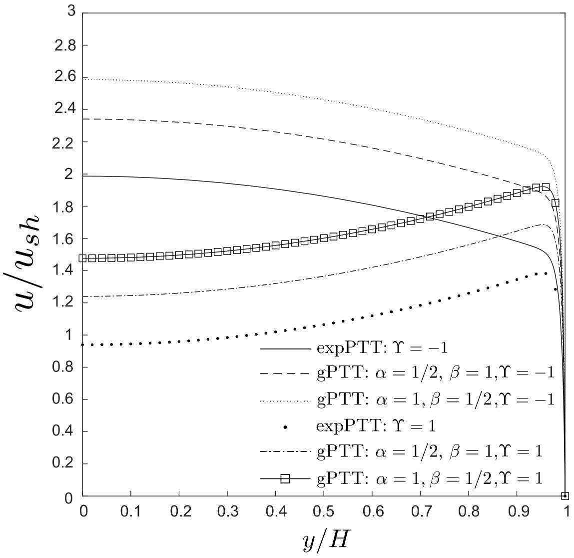

Figure 8: Velocity profiles obtained numerically for mixed EO/PD flow with $\Upsilon = -1$, $\Upsilon = 1$, $\bar{\kappa} = 100$ and $\varepsilon Wi^2 = 0.5$. The velocity profiles were obtained numerically using Eq. (23) and the cases expPTT correspond to $\alpha = \beta = 1$.

Fig. 8 shows velocity profiles obtained numerically for the EO+PD flow with $\Upsilon = -1$ and $\Upsilon = 1$, using the gPTT constitutive model. When $\alpha = 1$ and $\beta = 1$, the results match those presented in [12] for the exponential PTT model. Note that negative values of Υ correspond to a favourable pressure gradient, whereas $\Upsilon > 0$ corresponds to adverse pressure forcing. We can also see the effect of other independent dimensionless numbers on the transverse profile and the effect of parameters α and β in the velocity profiles. The quantities that previously increased the dimensionless flow rate in pure EO are also seen to increase the flow rate for EO+PD through enhanced shear-thinning effects, and in earlier works, much has been reported and discussed about other shear-thinning viscoelastic models (e.g., refer to [11] for the sPTT model, and to [32] for the PTT model).

4.3. The Influence of ξ on the Flow Stability and Flow Characteristics

For $\xi \neq 0$ a non-monotonic behaviour of the shear stress curve is obtained beyond a critical shear rate. By following the steps presented in [32] and [18] one obtains the following formula for the critical shear rate (at the wall), $\dot{\gamma}_c$:

$$\lambda\dot{\gamma}_c = \frac{\Gamma(\beta)}{\sqrt{\xi(2-\xi)}} E_{\alpha,\beta}\left(\frac{\varepsilon(1-\xi)}{\xi(2-\xi)}\right) \tag{29}$$

A comparison between the different stability formulas obtained for the different functions of the trace of the stress tensor is shown in [18].

To assess the influence of the ξ parameter on the fluid flow, we will now compare the results obtained with the analytical solution for pure EO flow with the results obtained from the numerical integration of Eq. (28). The numerical results were obtained using the Simpson's quadrature rule to approximate the integral and the Mathematica's predefined routine to calculate the Mittag-Leffler function. We will consider different values of Wi and ξ (ranging from 0.001 to 0.1).

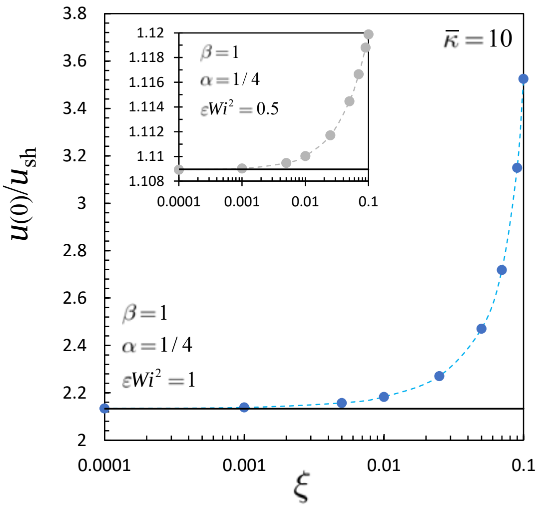

Figure 9: Maximum velocity at the centre of channel as a function of the ξ parameter. Pure EO flow with $\beta = 1$, $\alpha = 1/4$, $\bar{\kappa} = 10$ and $\varepsilon Wi^2 = 1$ and 0.5. The full line represents the asymptotic solution obtained for $\xi = 0$ (a constant solution) and the dashed line is a guide to the eye for the solution obtained numerically (represented by the symbols). The inset shows the results obtained for $\varepsilon Wi^2 = 0.5$.

Fig. 9 shows the maximum velocity at the centre of channel as a function of the ξ parameter, for pure EO flow with $\beta = 1$, $\alpha = 1/4$, $\bar{\kappa} = 10$ and $\varepsilon Wi^2 = 1$ and 0.5. The full line represents the solution obtained for $\xi = 0$ and the dashed line is a guide to the eye for the solution obtained numerically. The inset shows the results obtained for $\varepsilon Wi^2 = 0.5$.

The influence of ξ on the maximum velocity increases both with ξ and εWi^2, and very non-linearly with the latter. Indeed, for the case of $\varepsilon Wi^2 = 1$ we obtain increases in the maximum velocity up to 65% when ξ increases from 10^{-3} to 10^{-1}, whereas for $\varepsilon Wi^2 = 0.5$ the maximum velocity is only 1% higher. This difference is expected since the εWi^2 has a strong influence on the flow rate.

4.4. The Debye–Hückel approximation

By following the works [26, 27], we have that

$$\frac{\mathrm{d}^2\bar{\psi}}{\mathrm{d}\bar{y}^2} = \bar{\kappa}^2 \sinh(\bar{\psi}) \tag{30}$$

leading to,

$$\bar{\psi} = 4\mathrm{arctanh}\left(\tanh(\bar{\psi}_0/4)e^{\bar{\kappa}(\bar{y}-1)}\right). \tag{31}$$

The corresponding velocity profile can then be obtained by using a fourth-order Runge-Kutta method together with 20-30 parcels to approximate the Mittag-Leffler function. The velocity profile for each $\bar{y} \in [0, 1]$ is given by,

$$\bar{u}(\bar{y}) = -\int_{\bar{y}}^{1}\left(\frac{-\Gamma(\beta)}{\bar{\psi}_0}\frac{4\bar{\kappa}\tanh\left(\frac{\bar{\psi}_0}{4}\right)e^{\bar{\kappa}(z-1)}}{1-\tanh^2\left(\frac{\bar{\psi}_0}{4}\right)e^{2\bar{\kappa}(z-1)}}E_{\alpha,\beta}\left[\frac{2\varepsilon Wi^2}{\bar{\kappa}^2\bar{\psi}_0^2}\left(\frac{4\bar{\kappa}\tanh\left(\frac{\bar{\psi}_0}{4}\right)e^{\bar{\kappa}(z-1)}}{1-\tanh^2\left(\frac{\bar{\psi}_0}{4}\right)e^{2\bar{\kappa}(z-1)}}\right)^2\right]\right)\mathrm{d}z \tag{32}$$

We now compare in Fig. 10 the velocity profiles for a pure EO flow considering the Debye–Hückel approximation and the full solution obtained by Eq. (32), considering a fourth-order Runge-Kutta method together with 20-30 parcels to approximate the Mittag-Leffler function.

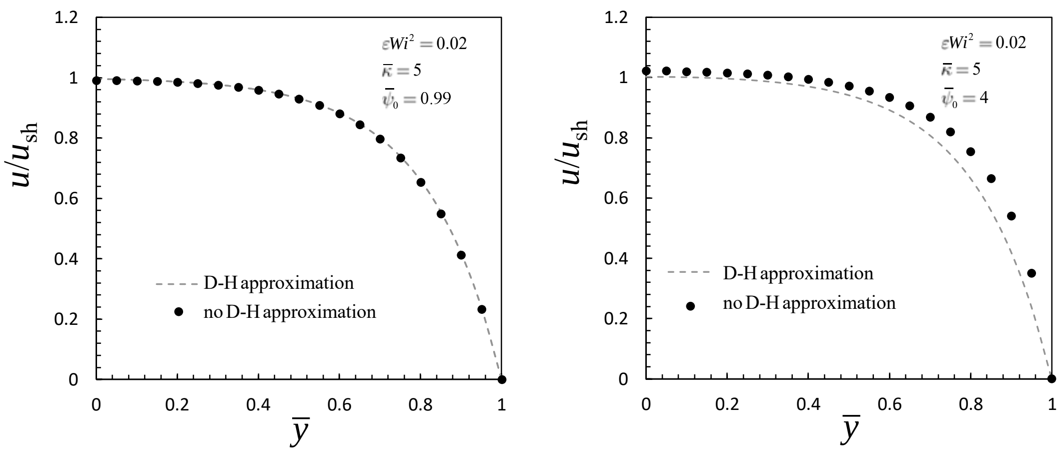

Figure 10: Comparison between velocity profiles for the exponential PTT model with $\bar{\kappa} = 5$ and $\varepsilon Wi^2 = 0.02$ for $\bar{\psi}_0 = 0.99$ and 4. Dashed line: solution obtained with the Debye–Hückel approximation; dots: solution obtained without the Debye–Hückel approximation (numerically solving Eq. (32)).

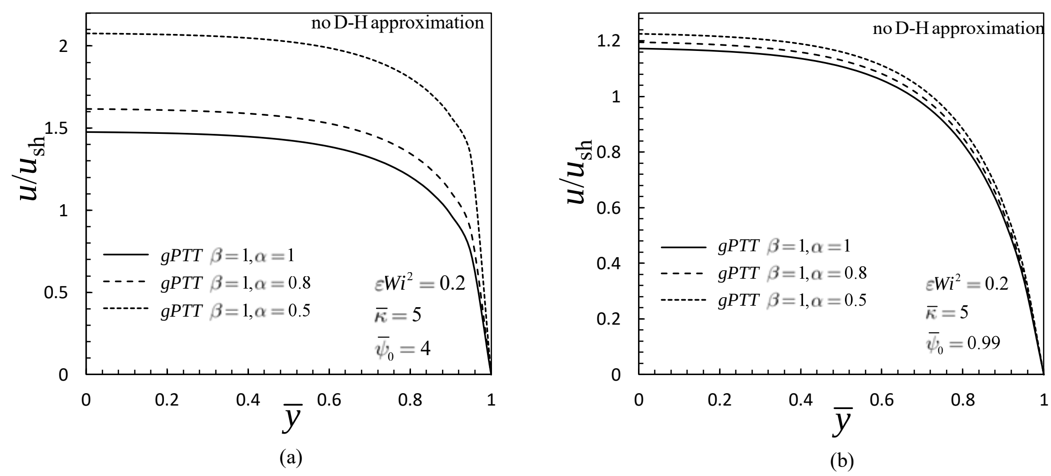

Figure 11: Velocity profiles obtained for both the exponential and gPTT models considering $\bar{\psi}_0 = 0.99$ and 4. Solutions obtained by numerically solving Eq. (32) with $\beta = 1$, $\alpha = 1,\ 0.8,\ 0.5$, $\bar{\kappa} = 5$ and $\varepsilon Wi^2 = 0.2$.

Fig. 10 shows the velocity profiles obtained for the exponential PTT model considering $\bar{\psi}_0 = 0.99$ and 4. We consider the solutions obtained with and without (numerically solving Eq. (32)) the Debye–Hückel approximation. It can be seen that for $\bar{\psi}_0 = 0.99$ the Debye–Hückel approximation is valid, while for $\bar{\psi}_0 = 4$ the two solutions become different, especially near the wall. Fig. 11 compares the velocity profiles obtained with both the exponential ($\alpha = 1$, $\beta = 1$) and gPTT models considering . The solutions were obtained by numerically solving Eq. (32) with $\beta = 1$, $\alpha = 1,\ 0.8,\ 0.5$, $\bar{\kappa} = 5$ and $\varepsilon Wi^2 = 0.2$. It is remarkable the influence of ψ_0 on the effect of coefficient α for the gPTT model. At low ψ_0 the maximum velocity increases only 1% with the decreasing of α whereas for higher ψ_0 there is a 50% increase in the maximum velocity(when compared with the velocity obtained for the exponential PTT model: $\alpha = \beta = 1$).

5. Conclusions

This work presented new analytical and semi-analytical solutions for electro-osmotic and mixed electro-osmotic/pressure-driven flows of a viscoelastic fluid modelled by the gPTT model, respectively. From these solutions, the influence of the model parameters on the velocity profile was assessed. The new model allows a broader description of flow behaviour than the more classical descriptions, and therefore it can be considered in modelling complex viscoelastic flows. Numerical solutions were also presented for high zeta potential. The analytical and numerical solutions presented in this work are helpful for validating CFD codes, and also allow a better understanding of the model behaviour in simple shear flows.

Acknowledgements

A.M. Ribau would like to thank FCT - Fundação para a Ciência e a Tecnologia, for financial support through scholarship SFRH/BD/143950/2019.
A.M. Ribau, A.M. Afonso, M.A. Alves and F.T Pinho also acknowledge FCT for financial support through projects UIDB/00532/2020 and UIDP/00532/2020 of CEFT (Centro de Estudos de Fenómenos de Transporte), and through PTDC/EMS-ENE/3362/2014 and POCI-01-0145-FEDER-016665 - funded by FEDER funds through COMPETE2020 - Programa Operacional Competitividade e Internacionalização (POCI) and by national funds through FCT.
L.L. Ferrás would also like to thank FCT for financial support through scholarship SFRH/BPD/100353/2014 and projects UIDB/00013/2020 and UIDP/00013/2020.
M.L. Morgado aknowledges funding by FCT through project UID/Multi/04621/2019 of CEMAT/IST-ID, Center for Computational and Stochastic Mathematics, Instituto Superior Técnico, University of Lisbon.
This work was partially supported by the Fundação para a Ciência e a Tecnologia (Portuguese Foundation for Science and Technology) through the project UIDB/00297/2020 (Centro de Matemática e Aplicações).
The authors also acknowledge financial support from COST Action CA15225, a network supported by COST (European Cooperation in Science and Technology).

References

[1] Bruus H., Theoretical Microfluidics, Oxford Master Series in Condensed Matter Physics (Oxford University Press, Oxford, UK, 2008).
[2] D. Burgreen and F. R. Nakache, Electrokinetic flow in ultrafine capillary slits, J. Phys. Chem. 68, 1084-1091 (1964).
[3] C. L. Rice and R. Whitehead, Electrokinetic flow in a narrow cylindrical capillary, J. Phys. Chem. 69, 4017-4024 (1964).
[4] S. Arulanandam and D. Li, Liquid transport in rectangular microchannels by electroosmotic pumping, Colloids Surf., A 161, 29 102 (2000)
[5] P. Dutta and A. Beskok, Analytical solution of combined electroosmotic/pressure driven flows in two-dimensional straight channels: Finite Debye layer effects, Anal. Chem. 73, 1979-1986 (2001)
[6] S. Das and S. Chakraborty, Analytical solutions for velocity, temperature and concentration distribution in electroosmotic microchannel flows of a non-Newtonian bio-fluid, Anal. Chim. Acta 559, 15-24 (2006)
[7] C. L. A. Berli and M. L. Olivares, Electrokinetic flow of non-Newtonian fluids in microchannels, J. Colloid Interface Sci. 320, 582-589 (2008)
[8] C. Zhao and C. Yang, An exact solution for electro-osmosis of non-Newtonian fluids in microchannels, J. Non-Newtonian Fluid Mech. 166, 1076-1079 (2012)
[9] C. Zhao and C. Yang, Electro-osmotic mobility of non-Newtonian fluids, Biomicrofluidics 5, 014110 (2011)
[10] Zhao, C., Yang, C., Adv. Colloid. Interf. Sci. 2013, 201 202, 94 108.
[11] Afonso, A. M., Alves, M. A., and Pinho, F. T., Analytical solution of mixed electro-osmotic/pressure driven viscoelastic fluids in microchannels. J. Non-Newtonian Fluid Mech., 2009. 159: p. 50-63.

[12] Ferrás, L.L., Afonso, A. M., Alves, M. A., Nóbrega, J. M. and Pinho, F. T., Electro-osmotic and pressure-driven flow of viscoelastic fluids in microchannels: Analytical and semi-analytical solutions. Physics of fluids, 2016. 28.

[13] P. Goswami, J. Chakraborty, A. Bandopadhyay, S. Chakraborty, Electrokinetically modulated peristaltic transport of power-law fluids, Microvascular Research 103 (2015) 41-54.

[14] S. Das, S. Chakraborty, Transverse electrodes for improved DNA hybridization in microchannels, AIChE Journal 53 (2007) 1086-1099.

[15] Bird, R. B., Armstrong, R. C., Hassager, O, Dynamics of polymeric liquids. Volume 1: fluid mechanics. A Wiley-Interscience Publication, John Wiley & Sons (1987).

[16] Phan-Thien, N. and R. Tanner, A new constitutive equation derived from network theory. Journal of Non-Newtonian Fluid Mechanics 2 (1977) 353-365.

[17] Phan-Thien, N., A Nonlinear Network Viscoelastic Model. Journal of Rheology 22 (1978) 259-283.

[18] Ferrás, L.L., Morgado, M.L., Rebelo, M., McKinley Gareth, H., Afonso, A.M., A Generalised Phan-Thien-Tanner Model. Journal of Non-Newtonian Fluid Mechanics, 2019. 269: p. 88-99.

[19] F. Del Giudice, G. D'Avino, F. Greco, I. De Santo, P.A. Netti, P.L. Maffettone, Rheometry-on-a-chip: measuring the relaxation time of a viscoelastic liquid through particle migration in microchannel flows. Lab on a Chip, 15(3) (2015) 783-792.

[20] S. Mukherjee, S.S. Das, J. Dhar, S. Chakraborty, S. DasGupta, Electroosmosis of viscoelastic fluids: Role of wall depletion layer. Langmuir, 33(43) (2017) 12046-12055.

[21] A. Zell, S. Gier, S. Rafai, C. Wagner, Is there a relation between the relaxation time measured in CaBER experiments and the first normal stress coefficient?. Journal of non-newtonian fluid mechanics, 165(19-20) (2010) 1265-1274.

[22] P.K. Mondal, U. Ghosh, A. Bandopadhyay, D DasGupta, S. Chakraborty, Pulsating electric field modulated contact line dynamics of immiscible binary systems in narrow confinements under an electrical double layer phenomenon. Soft Matter 10 (2014) 8512-8523.

[23] S. Mukherjee, S.S. Das, J. Dhar, S. Chakraborty, S. DasGupta, Electroosmosis of viscoelastic fluids: Role of wall depletion layer, Langmuir 33(43) (2017) 12046-12055.

[24] I. Borukhov, D. Andelman, H. Orland, Steric effects in electrolytes: A modified Poisson-Boltzmann equation. Physical review letters, 79(3) (1997) 435.

[25] M.Z. Bazant, K. Thornton, A. Ajdari, Diffuse-charge dynamics in electrochemical systems. Physical review E, 70(2) (2004) 021506.

[26] S. Mukherjee, P. Goswami, J. Dhar, S. Dasgupta, S. Chakraborty, Ion-size dependent electroosmosis of viscoelastic fluids in microfluidic channels with interfacial slip. Physics of Fluids, 29(7) (2017) 072002.

[27] A. Bandopadhyay, S. Chakraborty, Electrokinetically induced alterations in dynamic response of viscoelastic fluids in narrow confinements. Physical Review E, 85(5) (2012) 056302.

[28] Ribau, A.M., Ferrás, L.L., Morgado, M.L., Rebelo, M., Afonso, A. M., Semi-analytical solutions for the Poiseuille-Couette flow of a generalised Phan-Thien-Tanner fluid. Fluids, 2019. 4, 129.

[29] Ribau A. M., Ferrás L. L., Morgado M.L., Rebelo M. Afonso A. M., Analytical and numerical studies for slip flows of a generalised Phan-Thien–Tanner fluid. Z Angew Math Mech. 2020.

[30] Oliveira, P.J. and F.T. Pinho, Analytical solution for fully developed channel and pipe flow of Phan-Thien–Tanner fluids. Journal of Fluid Mechanics, 1999. 387: p. 271-280.

[31] Ferrás, L.L., Afonso, A.M., Alves, M.A., Nóbrega, J.M., Pinho, F.T., Annular flow of viscoelastic fluids: Analytical and numerical solutions. Journal of Non-Newtonian Fluid Mechanics, 2014. 212: p. 80-91.

[32] Dhinakaran, S., Afonso, A.M., Alves, M.A. and Pinho, F.T., Steady viscoelastic fluid flow between parallel plates under electro-osmotic forces: Phan-Thien–Tanner model. J. Colloid Interface Sci., 2010. 344: 513-520.

Appendices

Appendix A. Finite Sized Ionic Species

Note that the Boltzmann distribution breaks down when taking into account finite-sized ionic species. Therefore we obtained a new modified Poisson-Boltzmann equation for the ionic distribution [24–26] to take these effects into account. The corrected distribution is given by:

$$\frac{\mathrm{d}^2\psi}{\mathrm{d}y^2} = \frac{2n_0 ez}{\epsilon} \frac{\sinh\left(\frac{ez}{k_B T}\psi\right)}{1 - \Theta + \Theta\cosh\left(\frac{ez}{k_B T}\psi\right)}. \tag{A.1}$$

where Θ is the steric factor, representing the excluded volume effects owing to the finite size of the ionic species. This is a nonlinear differential equation, and therefore, in order to obtain the induced potential distribution the procedure used in [26] was followed.

By following the work of Mukherjee et al. [26], one can easily obtain the shear rate as a function of the zeta potential:

$$\frac{\mathrm{d}\bar{u}}{\mathrm{d}\bar{y}} = \frac{-\Gamma(\beta)}{\bar{\psi}_0}\frac{\mathrm{d}\bar{\psi}}{\mathrm{d}\bar{y}}E_{\alpha,\beta}\left[\frac{2\varepsilon Wi^2}{\bar{\kappa}^2\bar{\psi}_0^2}\left(\frac{\mathrm{d}\bar{\psi}}{\mathrm{d}\bar{y}}\right)^2\right], \tag{A.2}$$

where $\bar{\psi}_0 = \frac{ez\psi_0}{k_B T}$.

- For a low zeta potential, the size of the ionic species is negligible and the Debye–Hückel approximation applies. We obtain the solutions derived previously.
- For a high zeta potential [26, 27] we have that

$$\frac{\mathrm{d}^2\bar{\psi}}{\mathrm{d}\bar{y}^2} = \frac{\bar{\kappa}^2\sinh(\bar{\psi})}{1-\Theta+\Theta\cosh(\bar{\psi})} \approx \frac{\bar{\kappa}^2}{\Theta} \tag{A.3}$$

leading to (the boundary conditions are $\left.\frac{\mathrm{d}\bar{\psi}}{\mathrm{d}\bar{y}}\right|_{\bar{y}=0} = 0$ and $\bar{\psi}(1) = \bar{\psi}_0$),

$$\bar{\psi} = \bar{\psi}_0 + \frac{\bar{\kappa}^2(\bar{y}^2-1)}{2\Theta}. \tag{A.4}$$

The corresponding velocity profile can then be obtained by using a fourth-order Runge-Kutta method together with 20-30 parcels to approximate the Mittag-Leffler function. The velocity profile for each $\bar{y} \in [0,1]$ is given by,

$$\bar{u}(\bar{y}) = -\int_{\bar{y}}^{1}\frac{-\Gamma(\beta)}{\bar{\psi}_0}\frac{\bar{\kappa}^2 z}{\Theta}E_{\alpha,\beta}\left[\frac{2\varepsilon Wi^2}{\bar{\psi}_0^2}\left(\frac{\bar{\kappa}z}{\Theta}\right)^2\right]\mathrm{d}z \tag{A.5}$$

Appendix B. The High Zeta Potential and Steric effect

The higher the steric factor, the lower will be the induced transverse EDL field, and thus, a lower volumetric flow rate will be obtained. This effect is shown in Fig. B.12, where the velocity profiles obtained for both the exponential and gPTT models are plotted (considering $\Theta = 0.2$ and 0.25 and a high zeta potential $\bar{\psi}_0 = 4$).

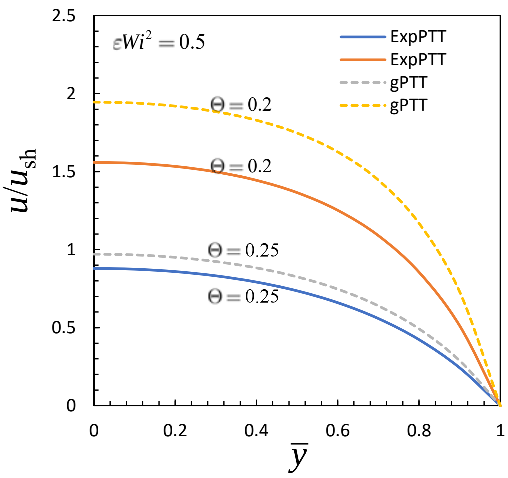

Figure B.12: Velocity profiles obtained for both the exponential and gPTT models considering $\Theta = 0.2$ and 0.25 and a high zeta potential ($\bar{\psi}_0 = 4$). Dashed line: Pure EO flow with $\beta = 1$, $\alpha = 0.8$; Full line: Pure EO flow with $\beta = 1$, $\alpha = 0.8$. $\bar{\kappa} = 1$ and $\varepsilon Wi^2 = 0.5$.

As expected, the gPTT model allows one to obtain a higher flow rate due to the higher rate of destruction of junctions in the polymer entanglements, resulting in a less restrictive fluid flow. Note also the nonlinear increase of the flow rate with decreasing α at constant Θ, showing the complex combination of rate of destruction of junctions and the size of the ions.